# Model study on $\Upsilon(nS)$ modification in small collision systems

Junlee Kim,[1] Jinjoo Seo,[2] Byungsik Hong,[3] Juhee Hong,[4] Eun-Joo Kim,[1] Yongsun Kim,[5] MinJung Kweon,[2] Su Houng Lee,[4] Sanghoon Lim,[6] and Jaebeom Park[3]

[1]*Division of Science Education, Jeonbuk National University, Jeonju 54896, South Korea*
[2]*Department of Physics, Inha University, Incheon 22212, South Korea*
[3]*Department of Physics, Korea University, Seoul 02841, South Korea*
[4]*Department of Physics and Institute of Physics and Applied Physics, Yonsei University, Seoul 03722, Korea*
[5]*Department of Physics, Sejong University, Seoul 05006, South Korea*
[6]*Department of Physics, Pusan National University, Busan 46241, South Korea*

(Received 2 October 2022; accepted 7 April 2023; published 4 May 2023)

Quarkonium production has been studied extensively in relativistic heavy-ion collision experiments to understand the properties of the quark-gluon plasma. The experimental results on the yield modification in heavy-ion collisions relative to that in $p+p$ collisions can be described by several models considering dissociation and regeneration effects. A yield modification beyond initial-state effects has also been observed in small collision systems such as $p+\mathrm{Au}$ and $p+\mathrm{Pb}$ collisions, but it is still premature to claim any hot medium effect. A model study in various small collision systems such as $p+p$, $p+\mathrm{Pb}$, $p+\mathrm{O}$, and $\mathrm{O}+\mathrm{O}$ collisions will help quantitatively the understanding of nuclear effects on the $\Upsilon(nS)$ production. A theoretical calculation considering the gluo-dissociation and inelastic parton scattering for dissociation, and their inverse reaction for regeneration, reasonably describes the modification of $\Upsilon(1S)$ in $\mathrm{Pb}+\mathrm{Pb}$ collisions. Based on this calculation, a Monte Carlo simulation considering the dissociation effect is developed to more realistically incorporate the medium produced in heavy-ion collisions with event-by-event initial collision geometry and hydrodynamic evolution. We extend this framework to small systems to study the medium effects. In this work, we quantify the nuclear modification factor of $\Upsilon(nS)$ as a function of charged particle multiplicity ($dN_{ch}/d\eta$) and transverse momentum. We also calculate the elliptic flow of $\Upsilon(nS)$ in small collision systems.

DOI: 10.1103/PhysRevC.107.054905

## I. INTRODUCTION

Quarkonia have long been considered as key probes to study the strongly interacting matter consisting of deconfined quarks and gluons, the quark-gluon plasma (QGP), produced in high-energy heavy-ion collisions [1–5]. Quarkonium states are produced at the early stages of the collision via hard parton scatterings, thus experiencing the full space-time evolution of the medium. Also, their spectral functions are modified due to color screening [4,5] and interactions with medium constituents such as gluo-dissociation or Landau damping [6–8]. Consequently, the quarkonium yields are expected to be suppressed in heavy ion collisions with respect to expectations from proton-proton ($p+p$) data, following the order of their binding energies. On the other hand, the yields of quarkonia can be enhanced in the presence of the QGP by recombination processes of uncorrelated as well as correlated quarks [9–12].

The modification of the quarkonium yields have been studied by various experiments at the BNL Relativistic Heavy Ion Collder (RHIC) and the CERN Large Hadron Collider (LHC) using the nuclear modification factor quantified as the yield ratio in nucleus-nucleus collisions ($A+A$) to that in $p+p$ collisions scaled by the average number of binary $NN$ collisions [13–20]. One of the most remarkable signatures is the ordered suppression of $\Upsilon(1S)$, $\Upsilon(2S)$, and $\Upsilon(3S)$ mesons by their binding energies reported at the LHC [16,18–20].

To better understand the in-medium effects of quarkonia in $A+A$ collisions in a sophisticated way, it is important to study the "cold nuclear matter" (CNM) effects, which are typically probed using proton-nucleus ($p+A$) collisions. Modification of parton distribution functions in the nucleus [21], energy loss [22] or nucleus absorption [23,24], and interactions with comoving particles [25–27] are examples of CNM effects. On the other hand, various experiments have reported capital results, suggesting a QGP-like behavior of the created medium also in smaller collision systems, such as the observation of long-range collective azimuthal correlations in high multiplicity regions [28–38]. Therefore, sophisticated phenomenological studies in such interactions have become a subject that is sensitive to understanding the quarkonium production in small collision systems.

In this paper, we report a detailed study of the in-medium effects for $\Upsilon(1S)$, $\Upsilon(2S)$, and $\Upsilon(3S)$ mesons in proton-lead ($p+\mathrm{Pb}$), proton-oxygen ($p+\mathrm{O}$), and oxygen-oxygen (O+O) collisions. Theoretical calculations for dissociation of $\Upsilon(nS)$ [39] are incorporated with the SONIC framework [40] to describe the time evolution of the medium. The dissociation component is constraint in potential nonrelativistic QCD (pNRQCD) limits, and coupled into the Boltzmann equation. The

 

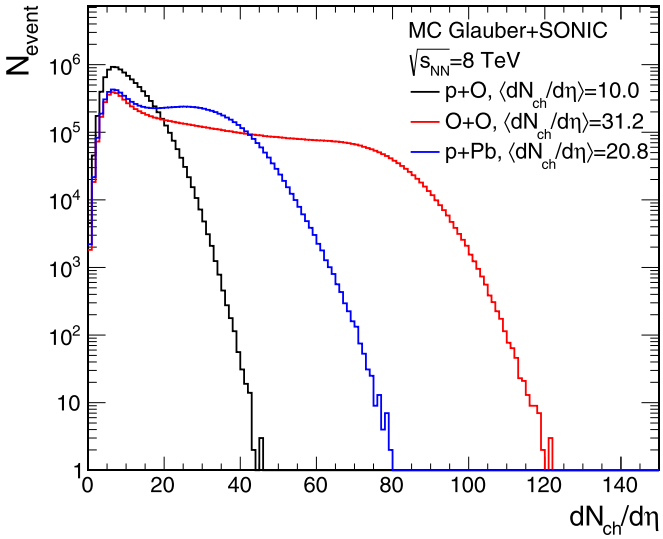


FIG. 1. Charged particle multiplicity distribution in $p+\mathrm{O}$, O+O, and $p+\mathrm{Pb}$ collisions at $\sqrt{s_{NN}} = 8$ TeV from SONIC.

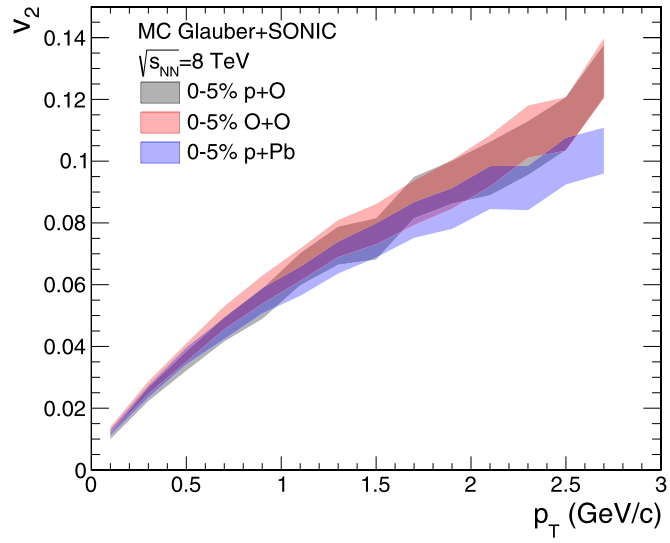


FIG. 2. Elliptic flow as a function of $p_T$ for charged particles in 0–5% central $p+\mathrm{O}$, O+O, and $p+\mathrm{Pb}$ collisions at $\sqrt{s_{NN}} = 8$ TeV from SONIC.

thermal width is calculated based on hard thermal loop (HTL) perturbation theory using the Bethe-Salpeter amplitude. We report the nuclear modification factors and the second-order Fourier coefficient ($v_2$) of the azimuthal distribution of $\Upsilon(nS)$ mesons in $p+\mathrm{Pb}$, $p+\mathrm{O}$, and O+O collisions, and the contribution of feed-down from higher excited states is considered to compare with the experimental data properly. For the demonstration of the framework, we also present the results in Pb+Pb collisions and compare them with the experimental results.

## II. SIMULATION FRAMEWORK

The simulation framework, Simulation for Heavy IoN Collision with Heavy-quark and ONia (SHINCHON), is composed of two parts, hydrodynamics simulation for background medium and medium response of quarkonia. For the first part, we follow the procedure described in Ref. [41]. Initial energy density in the transverse plane of nucleus-nucleus or proton-nucleus collisions is obtained with the Monte Carlo Glauber (MC-Glauber) framework [42]. In MC-Glauber, a nucleon-nucleon inelastic cross section of 72 mb [43] is employed for small system collisions at $\sqrt{s_{NN}} = 8$ TeV at the LHC. A Gaussian of width $\sigma = 0.4$ fm is used to describe the energy deposition of each nucleon participating in at least one inelastic collision. The deposited energy distribution from all wounded nucleons in each event is converted into energy density for the hydrodynamic simulation (SONIC). A single scale factor is used for all events in a certain collision system, and the scale factor is determined to match the charged particle multiplicity ($dN_{ch}/d\eta$) at midrapidity in $p+\mathrm{Pb}$ collisions at $\sqrt{s_{NN}} = 8.16$ TeV [44,45]. The same scale factor is used for $p+\mathrm{O}$ and O+O collisions at $\sqrt{s_{NN}} = 8$ TeV by assuming that the scale factor does not change much in collision systems with a similar number of participants.

Figure 1 shows the charged particle multiplicity distributions of unbiased (0–100%) $p+\mathrm{O}$, O+O, and $p+\mathrm{Pb}$ collisions at $\sqrt{s_{NN}} = 8$ TeV from SONIC. The mean charged particle multiplicities for $p+\mathrm{O}$ and O+O with the scale factor obtained from $p+\mathrm{Pb}$ collisions are 10.0 and 31.2, respectively. We also check the elliptic flow of charged particle in 0–5% high multiplicity events as shown in Fig. 2, and the $p+\mathrm{Pb}$ result is slightly lower than $p+\mathrm{O}$ and O+O results at higher $p_T$. Note that we use a shear viscosity to entropy density ratio of 0.08 and a bulk viscosity ratio of zero in the SONIC calculations. There are other frameworks for initial conditions [46,47], but we use only the MC-Glauber initial condition as a simple case in this study.

During the SONIC simulation, temperature distributions at multiple time steps are stored for medium response of upsilons. At the beginning of the second part, we generate $\Upsilon(nS)$ mesons, and the $x$ and $y$ positions are determined based on the initial energy density distribution. We used a Tsallis fit to the $p_T$ distribution of $\Upsilon(1S)$ in $\sqrt{s} = 5.02$ TeV [16] to sample $p_T$ of upsilons, and $p_x$ and $p_y$ are determined based on a randomly assigned azimuthal angle. We performed a systematic study using two $p_T$ distributions of $\Upsilon(1S)$ from PYTHIA8 [48] at $\sqrt{s} = 5.02$ and 8 TeV. The mean $p_T$ at the two energies differ by 5%, and the effect on the nuclear modification factor and elliptic flow is negligible. The medium response is simulated based on the procedure described in Ref. [39]. The fraction of survived upsilons for a certain time step ($\Delta t$) is calculated as

$$\frac{N(t+\Delta t, p_T)}{N(t, p_T)} = e^{-\int_t^{t+\Delta t} dt' \Gamma_{\mathrm{diss}}(t', p_T)}, \tag{1}$$

where $\Gamma_{\mathrm{diss}}$ is the thermal width depending on the medium temperature and upsilon $p_T$, and $\Delta t$ is set to 0.02 fm/$c$ in the hydrodynamic simulation. The medium temperature is from the SONIC simulation according to $x$, $y$, and $t$ values. The temperature in which the quarkonium's in-medium binding energy reaches zero, i.e., dissociation temperature, is set as 600, 240, and 190 MeV for $\Upsilon(1S)$, $\Upsilon(2S)$, and $\Upsilon(3S)$, respectively [49,50]. The thermal width from numerical calculations

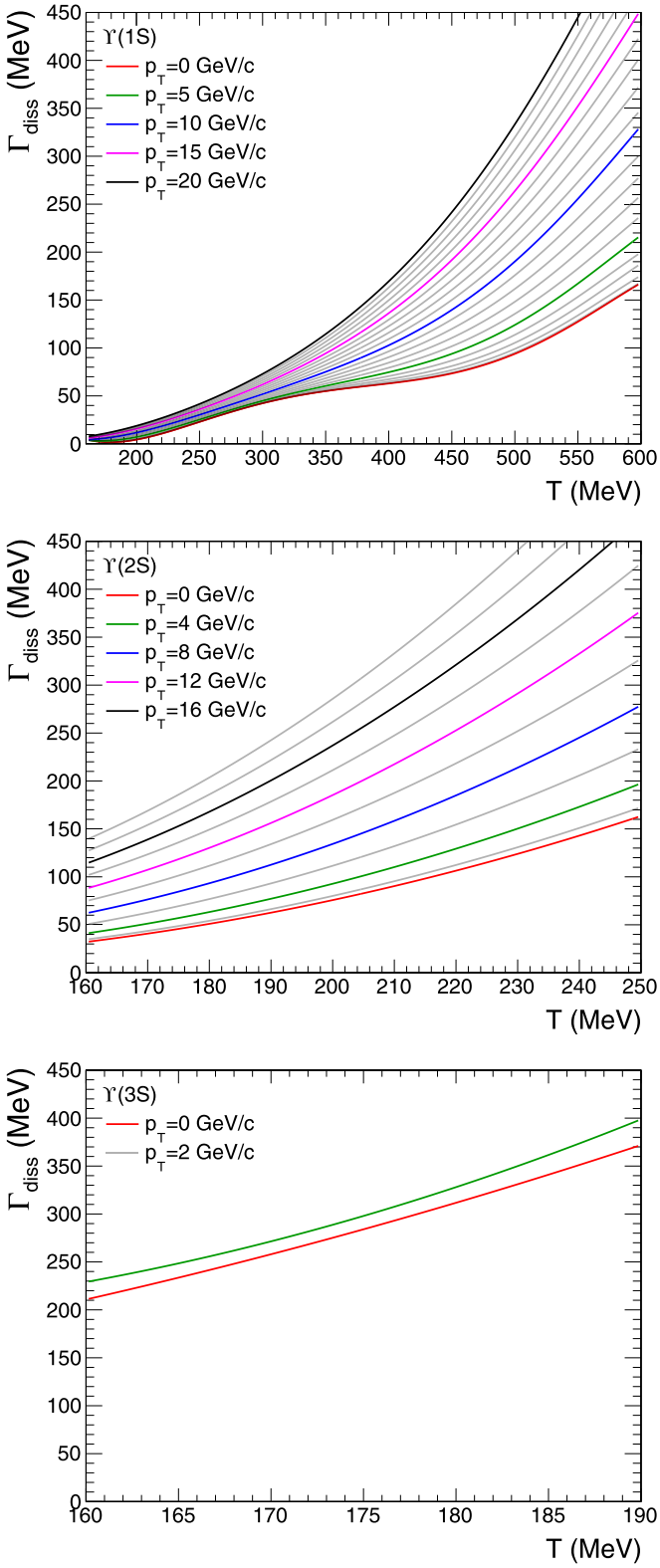


FIG. 3. Thermal width as a function of temperature for different $p_T$ of $\Upsilon(1S)$ (top), $\Upsilon(2S)$ (middle), and $\Upsilon(3S)$ (bottom).

considering gluo-dissociation and inelastic parton scattering is obtained from Ref. [39]. Figure 3 shows thermal width as function of temperature for $\Upsilon(1S)$ (left), $\Upsilon(2S)$ (middle), and $\Upsilon(3S)$ (right), and each line represents a distribution for different $p_T$. Gray lines represent distributions for $p_T$ between those indicated in the legend. Thermal width generally increases with $p_T$, and is larger for excited states. Note that thermal width for $\Upsilon(3S)$ is obtained in a limited $p_T$ range, so we estimated values for $p_T > 2$ GeV/$c$ using the $p_T$ dependence of $\Upsilon(2S)$ as

$$\Gamma^{\Upsilon(3S)}_{\rm diss}(p_T) = \Gamma^{\Upsilon(3S)}_{\rm diss}(2\ {\rm GeV}/c)\frac{\Gamma^{\Upsilon(2S)}_{\rm diss}(p_T)}{\Gamma^{\Upsilon(2S)}_{\rm diss}(2\ {\rm GeV}/c)}. \quad (2)$$

A different formation time ($\tau_{\rm form}$) of each state is used, 0.5, 1.0, and 1.5 for $\Upsilon(1S)$, $\Upsilon(2S)$, and $\Upsilon(3S)$, respectively, based on values in Ref. [51]. We do not consider dissociation at the preresonance stage, so the medium response on the $\Upsilon$ states is turned off for $\tau < \gamma\tau_{\rm form}$, where $\gamma$ is the Lorentz factor. We found that the overall medium response is sensitive to the choice of the formation time and preresonance response. The setting that can well reproduce heavy-ion results is used for small systems consistently. After incorporating the regeneration effect in heavy-ion collisions, a detailed systematic study will be performed later.

In each time step after the formation time, a survival rate is calculated for each $\Upsilon$ based on Eq. (1), and the $\Upsilon$ is removed when a random number from the uniform distribution within 0–1 is greater than the survival rate. If the $\Upsilon$ survives, the position for the next time step is calculated based on the momentum and time step ($\Delta t$). We repeat the survival rate calculation with a different temperature at the new position until the temperature is lower than a critical temperature of 170 MeV. For the simulation results presented in later sections, we use 1000 events for MC-Glauber and SONIC. The number of generated $\Upsilon(nS)$ for a certain event scales with the number of inelastic collisions from MC-Glauber. In this study, we do not consider a contribution from the regeneration effect, which is not expected to be significant in small collision systems. In addition, there could be other nuclear effects such as modification of parton density, initial-state energy loss, and other final-state effects, but we focus on evaluating the dissociation effect.

### A. Nuclear modification factor

The nuclear modification factors ($R_{pA}$ and $R_{AA}$) are defined as the ratios of the production cross sections of $\Upsilon$ mesons in $p+A$ and $A+A$ collisions to the expected cross sections extrapolated from $p+p$ collisions. To make an equivalent comparison, we took the ratio of generated to surviving numbers of $\Upsilon$'s in the full medium response simulation as the nuclear modification factor.

### B. Elliptic flow

The elliptic flow ($v_2$) is calculated from the azimuthal angle distribution of survived $\Upsilon(nS)$ with respect to the event plane angle,

$$\frac{dN}{d(\phi-\Psi)} \propto 1 + 2v_2(p_T)\cos[2(\phi-\Psi)],$$

where $\phi$ is the azimuthal angle of the $\Upsilon(nS)$, and $\Psi$ is the event plane angle. The event plane angle for each event is

calculated with the initial energy density profile from MC-Glauber.

### C. Feed-down correction

To simulate the medium response of inclusive bottomonium production, the contributions from feed-down decays, i.e., decays from higher excited states, need to be carefully considered. Here we consider only strong or electromagnetic decay modes of excited states in the feed-down decays, as the decays from $H$, $Z$, and $W$ bosons to $\Upsilon$ states have negligible effects to the inclusive yields. In general, the feed-down component from a $Q_m$ state to a $Q_n$ state ($Q_m$ being a higher excited state) can be calculated as

$$\mathcal{F}_{Q_n}^{Q_m} = \mathcal{B}(Q_m \to Q_n)\frac{\sigma_{Q_m}}{\sigma_{Q_n}}, \tag{3}$$

where $\mathcal{B}$ denotes the branching ratio of $Q_m$ into $Q_n$, and $\sigma_Q$ refers to the cross section of the corresponding state. We used publish experimental data in $p+p$ collisions at the LHC by CMS [52] and LHCb [53,54] Collaborations to estimate the feed-down fraction. Figure 4 shows the feed-down fraction from higher excited states for each $\Upsilon(1S)$, $\Upsilon(2S)$, and $\Upsilon(3S)$ state. The feed-down fractions from CMS are calculated using the presented cross section ratios multiplied by the Particle Data Group (PDG) world-average branching ratios [55] as in Eq. (3). The data points of each feed-down component are fitted with an empirical function and their sum is drawn as the black solid line, which is the total amount of feed-down fraction for the given $\Upsilon$ state. For $\Upsilon(2S)$ and $\Upsilon(3S)$, the fit function is parametrized to be the same as for the $P$-wave state feed-down function of $\Upsilon(1S)$ because of the absence of experimental measurements at low $p_T$. The function is scaled to match the average value of measured feed-down fraction at high $p_T$ for each $\Upsilon(2S)$ and $\Upsilon(3S)$. Note that the feed-down fractions from $\chi_b$ states in recent pNRQCD calculations also show a similar $p_T$ dependence for the three $\Upsilon$ states at $p_T > 15$ GeV/$c$ [56].

The feed-down contribution for the nuclear modification factor and elliptic flow of inclusive $\Upsilon(nS)$ is considered by calculating a weighted average of the quantities for possible states as

$$R_n(p_T) = \sum_i R_i(p_T)\mathcal{F}_{Q_n}^{Q_i}(p_T),$$

where $R_n$ is the weighted averaged value for a certain $\Upsilon(nS)$ state, $R_i$ is the value for a certain state contributing the the $\Upsilon(nS)$ state, and $\mathcal{F}_{Q_n}^{Q_i}$ is the feed-down fraction. The effect of possible $p_T$ shifts by the decays are ignored as the daughter particle carries mostly the mother $\Upsilon$'s momentum because of their similar masses. Since we do not have the nuclear modification factor and elliptic flow for $\chi_b$ states, it is assumed that $R_{\Upsilon(2S)} \approx R_{\chi_b(1P)}$ and $R_{\Upsilon(3S)} \approx R_{\chi_b(2P)} \approx R_{\chi_b(3P)}$ like the study in Ref. [39]. For a systematic study, we estimate nuclear modification factors for $\chi_b$ states using nuclear modification factor for prompt $\Upsilon(nS)$ states and binding energies listed

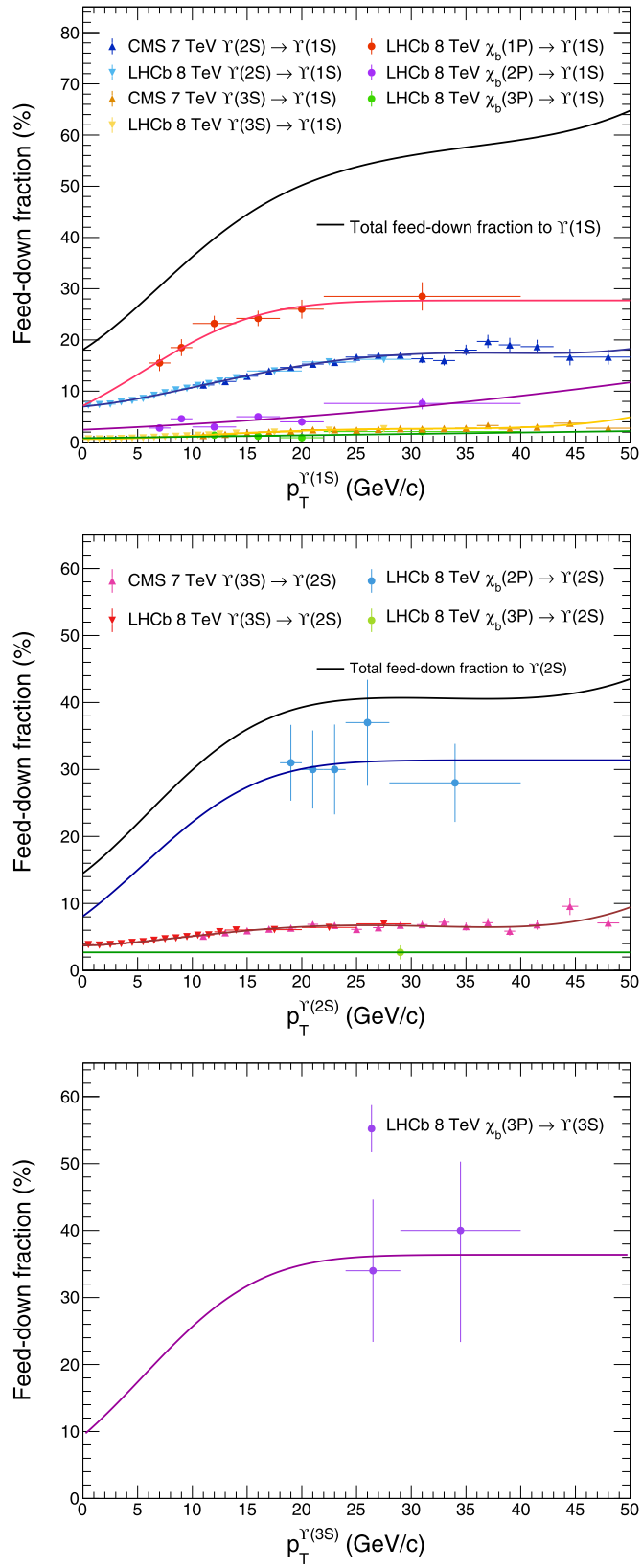


FIG. 4. Feed-down fractions for $\Upsilon(1S)$ (top), $\Upsilon(2S)$ (middle), and $\Upsilon(3S)$ (bottom) states.

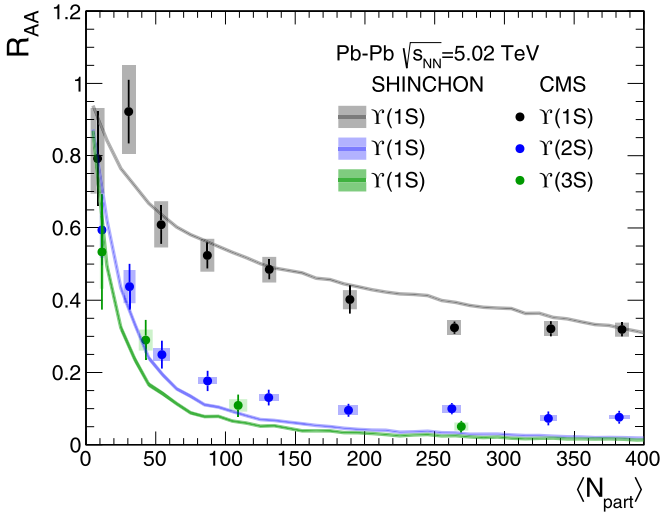


FIG. 5. Calculated $R_{AA}$ for $\Upsilon$ states as a function of $\langle N_{\rm part}\rangle$ in Pb+Pb collisions at $\sqrt{s_{NN}} = 5.02$ TeV. The uncertainties of the curves represent the statistical uncertainty to the corresponding simulated events. The data points are taken from results by CMS [16,20].

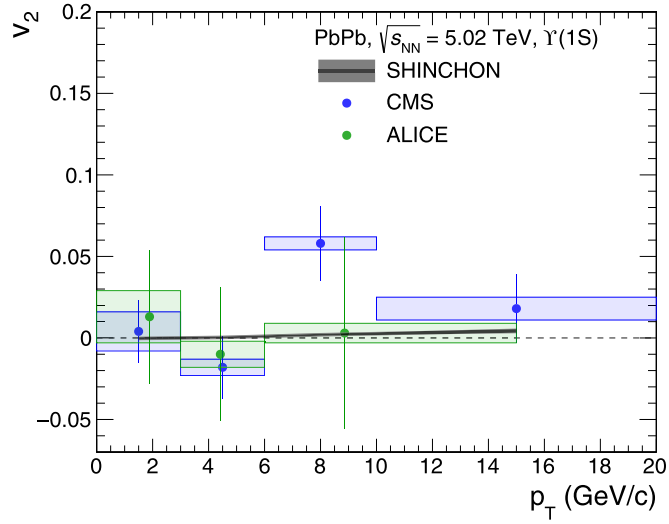


FIG. 6. Calculated $v_2$ for $\Upsilon(1S)$ as a function of $p_T$ in Pb+Pb collisions at $\sqrt{s_{NN}} = 5.02$ TeV. The uncertainties of the curves represent the statistical uncertainty to the corresponding simulated events. The data points are taken from results by ALICE [57] and CMS [58].

in Ref. [50]. The relative difference in nuclear modification factors with the feed-down correction is less than 5%.

## III. RESULTS AND DISCUSSIONS

This section presents and discuss the obtained results of nuclear modification factors ($R_{pA}$, $R_{AA}$) and elliptic flow ($v_2$) for $\Upsilon(1S)$, $\Upsilon(2S)$, and $\Upsilon(3S)$ mesons in $p+$Pb, $p+$O, and O+O collisions at $\sqrt{s_{NN}} = 8$ TeV. The performance of our framework is tested in nucleus-nucleus collisions and compared with the experimental data from the LHC as described in Sec. III A. The results of the nuclear modification factors and $v_2$ in the three small collision systems are shown and discussed in Secs. III B and III C, respectively. For all results, the uncertainty represents the statistical uncertainty that arises from the number of generated events. Also, the feed-down corrections are applied in all calculations as described in Sec. II C.

### A. Framework demonstration in Pb+Pb

The medium response of the full simulation is demonstrated in Pb+Pb collisions at $\sqrt{s_{NN}} = 5.02$ TeV. Figure 5 shows the $R_{AA}$ curves for $\Upsilon(1S)$, $\Upsilon(2S)$, and $\Upsilon(3S)$ as a function of $\langle N_{\rm part}\rangle$ in Pb+Pb collision at $\sqrt{s_{NN}} = 5.02$ TeV together with the measurements from CMS [16,20]. The calculations agree well with the experimental data for $\Upsilon(1S)$ after applying feed-down corrections, while this correction seems to have restricted effects for $\Upsilon(2S)$ and $\Upsilon(3S)$. The results of the excited $\Upsilon$ states show consistency with data in peripheral collisions, although deviations are found towards central Pb+Pb collisions. The discrepancy in central collisions might be present due to the exclusion of recombination processes in this paper, and is expected to be more prominent at large $\langle N_{\rm part}\rangle$ values.

Figure 6 shows the computed results of $v_2$ as a function of $p_T$ for $\Upsilon(1S)$ mesons under the same conditions for the Pb+Pb $R_{AA}$ calculations. The results indicate very small $v_2$ values in Pb+Pb collisions for $\Upsilon(1S)$ mesons, which is consistent with the measurements from ALICE [57] and CMS [58].

### B. Nuclear modification factor

The calculated nuclear modification factors as a function of $dN_{ch}/d\eta$ for $\Upsilon(1S)$, $\Upsilon(2S)$, and $\Upsilon(3S)$ mesons in $p+$Pb, $p+$O, and O+O collisions at $\sqrt{s_{NN}} = 8$ TeV are shown in Fig. 7. The nuclear modification factor shows a gradual decrease with increasing event multiplicity for all three $\Upsilon$ states in all three collision systems. Also, the amount of suppression towards higher multiplicity events is found to be sequentially ordered following the magnitude of the corresponding $\Upsilon$ binding energy.

To diagnose the strength of modification among different collision systems, the nuclear modification factors are separately displayed for each $\Upsilon$ state as shown in Fig. 8. In the low multiplicity region ($dN_{ch}/d\eta < 25$), the suppression level of $\Upsilon$ states is found to be similar in $p+$Pb and $p+$O collisions, while slightly less suppression is seen in O+O collisions, in particular for $\Upsilon(2S)$ and $\Upsilon(3S)$. Despite the medium size in O+O collisions being the largest and that in $p+$O collisions the smallest, the amount of suppression is not proportional to the size of the created system. The fact that the system size is larger in a given multiplicity event rather implies a smaller energy density of the medium. Therefore, we conclude that the weaker suppression in O+O collisions accounts for the smaller energy density compared to $p+$O and $p+$Pb collisions. In the higher multiplicity region, where the results in $p+$Pb and O+O collisions are compared, $\Upsilon$ states are more strongly suppressed in $p+$Pb collisions than

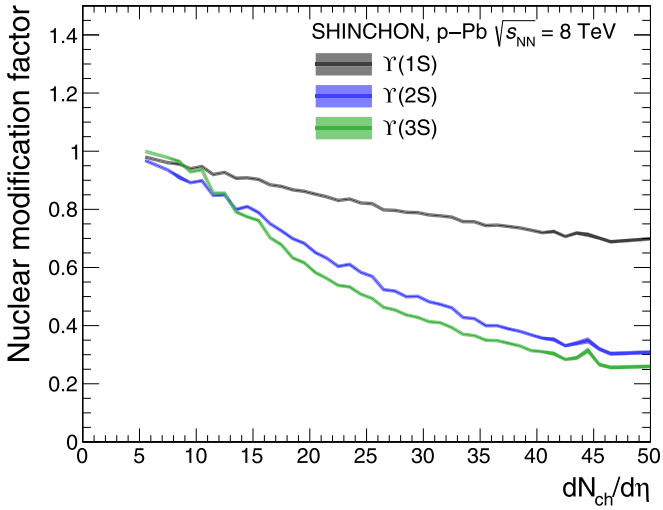


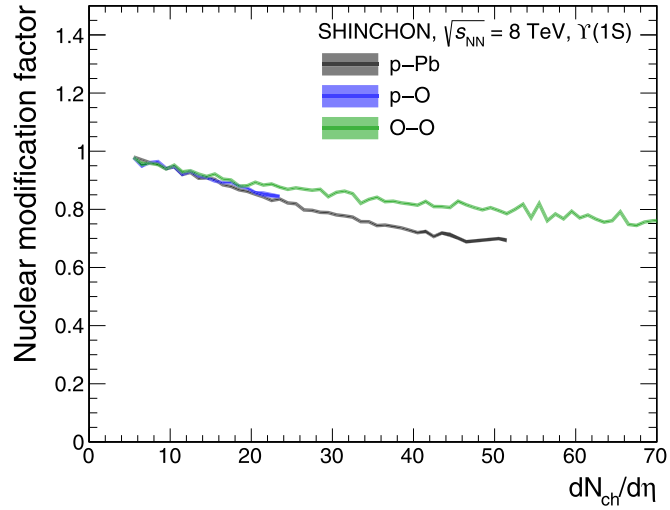


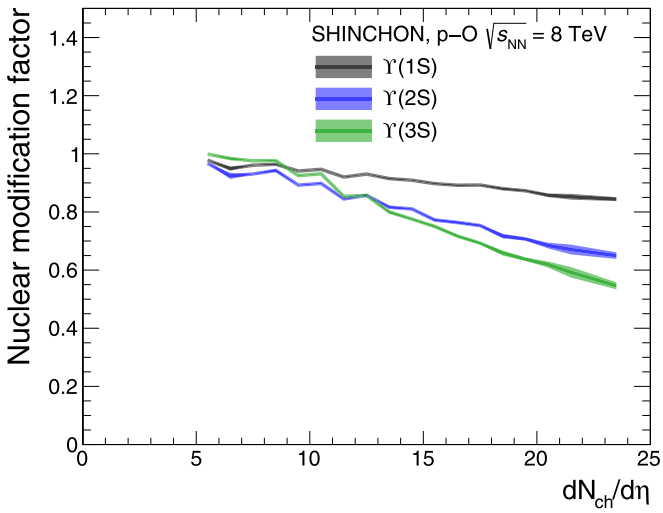


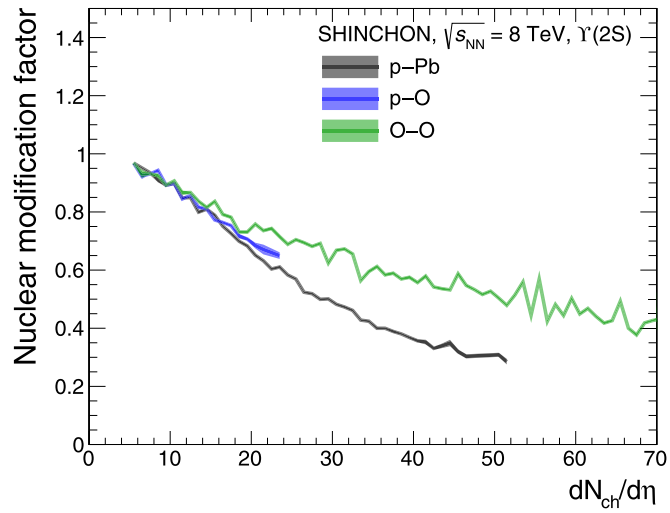


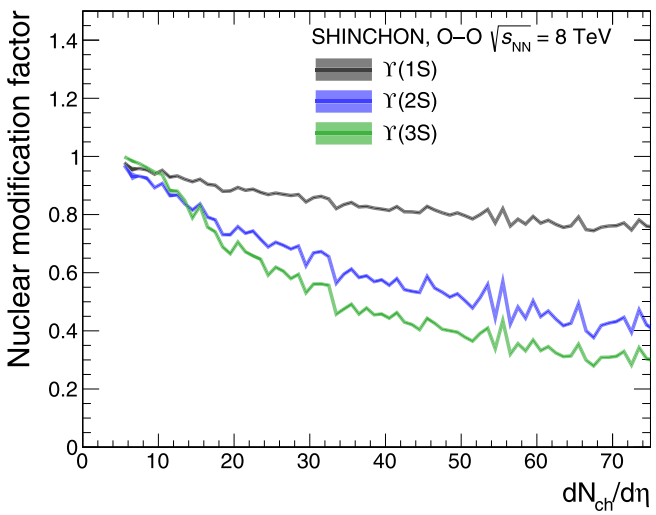


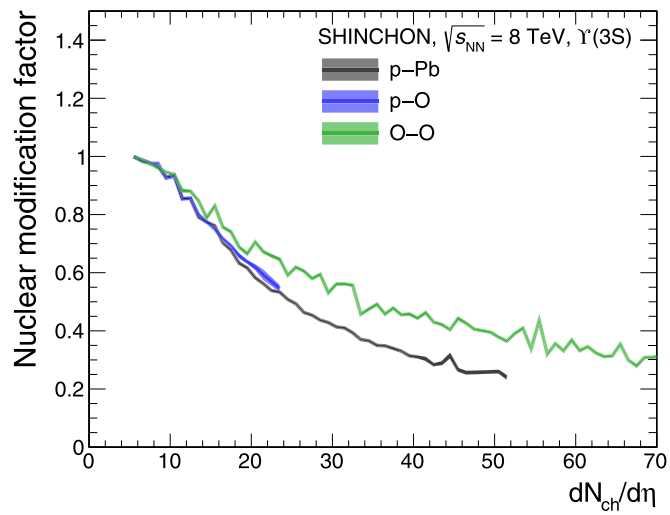


FIG. 7. Nuclear modification factors for $\Upsilon(1S)$, $\Upsilon(2S)$, and $\Upsilon(3S)$ as a function of $dN_{ch}/d\eta$ in $p+\mathrm{Pb}$ (top), $p+\mathrm{O}$ (middle), and O+O (bottom) collisions at $\sqrt{s_{NN}} = 8$ TeV. The uncertainties represent the statistical uncertainty to the corresponding simulated events.

FIG. 8. Calculated nuclear modification factor as a function of $dN_{ch}/d\eta$ in $p+\mathrm{Pb}$, $p+\mathrm{O}$, and O+O collisions at $\sqrt{s_{NN}} = 8$ TeV each for $\Upsilon(1S)$ (top), $\Upsilon(2S)$ (middle), $\Upsilon(3S)$ (bottom). The uncertainties represent the statistical uncertainty to the corresponding simulated events.

in O+O collisions, which is consistent with the finding at low multiplicity for the same reason.

For a more detailed look, the nuclear modification factors are presented as a function of charged particle density in Fig. 9; the charged particle density is calculated with the transverse area of initial collision geometry defined as

$$S_T = \pi\sqrt{\langle x^2\rangle\langle y^2\rangle - \langle xy\rangle^2}, \tag{4}$$

where $x$ and $y$ are the spatial coordinates of the participating nucleons from MC-Glauber. In each collision system, the amount of suppression increases with increasing charged particle density. In O+O collisions, a stronger suppression is seen than in $p+\mathrm{O}$ and $p+\mathrm{Pb}$ collisions at the same charged particle density because the size of the system and the duration of hydrodynamic evolution are larger. In the comparison between $p+\mathrm{O}$ and $p+\mathrm{Pb}$ collisions, a similar nuclear modification is seen. The small difference at higher density is also related to a slightly larger system size in $p+\mathrm{Pb}$ collisions.

Figure 10 shows the same quantities presented as a function of $p_T$. The ordering of the nuclear modification factors is similar at low $p_T$ as in Fig. 8, but found to be reversed between $p+\mathrm{Pb}$ and O+O collisions at high $p_T$. Since the formation time of the $\Upsilon$ states is delayed towards the higher $p_T$ region, the effective interaction time with the medium is also reduced. This effect is more prominent in $p+\mathrm{Pb}$ collisions because of the smaller initial medium size. The relation between the medium size and energy density affects the $\Upsilon$ suppression in the opposite direction for low and high $p_T$. These results show that the shape of the $p_T$-dependent nuclear modification factor is sensitive to the formation time and initial collision geometry.

We also compare our calculations with measured data by CMS in $p+\mathrm{Pb}$ collisions at $\sqrt{s_{NN}} = 5.02$ TeV [59], as shown in Fig. 11. The results are in good agreement with data for $\Upsilon(1S)$, whereas deviations are seen for $\Upsilon(2S)$ and $\Upsilon(3S)$. Note that our $R_{pA}$ values are for 8 TeV, in which the average multiplicity is about 15% higher than that at 5.02 TeV [44]. This difference affects the modification of $\Upsilon$ yields more significantly at low $p_T$, where they mostly experience the full medium evolution. Although the mean $p_T$ of the highest $p_T$ bin of the CMS measurements for the $\Upsilon(2S)$ and $\Upsilon(3S)$ meson is expected to be slightly lower than the center of the bin, our calculations still overshoot the experimental data. As discussed in Fig. 10, this disagreement is possibly related to the formation time and initial collision geometry. Note that initial-state model calculations considering modification of nuclear parton distribution functions and energy loss show about 10% suppression of $\Upsilon(1S)$ at midrapidity [21,44,60]. Since initial-state effects are expected to be similar for $\Upsilon(1S)$ and $\Upsilon(2S)$, one can take a ratio of the nuclear modification factors to cancel the initial-state effects as shown in the bottom panel of Fig. 11. The relative suppression of $\Upsilon(2S)$ is stronger in the model than in the CMS results.

### C. Elliptic flow

$v_2$ is calculated in the same setting as in the calculation for the nuclear modification factors in Sec. III B, and is shown

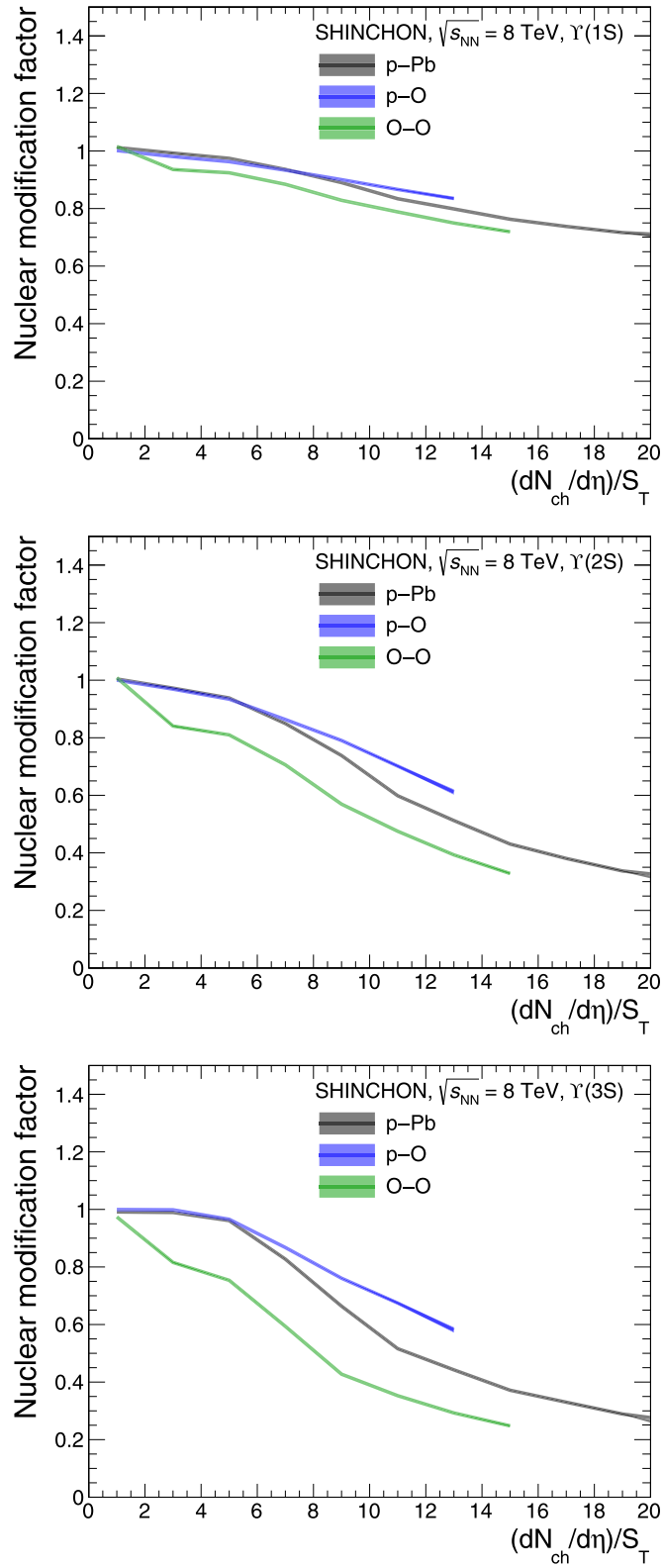


FIG. 9. Calculated nuclear modification factor as a function of $(dN_{ch}/d\eta)/S_T$ in $p+\mathrm{Pb}$, $p+\mathrm{O}$, and O+O collisions at $\sqrt{s_{NN}} =$ 8 TeV each for $\Upsilon(1S)$ (top), $\Upsilon(2S)$ (middle), $\Upsilon(3S)$ (bottom). The uncertainties represent the statistical uncertainty to the corresponding simulated events.

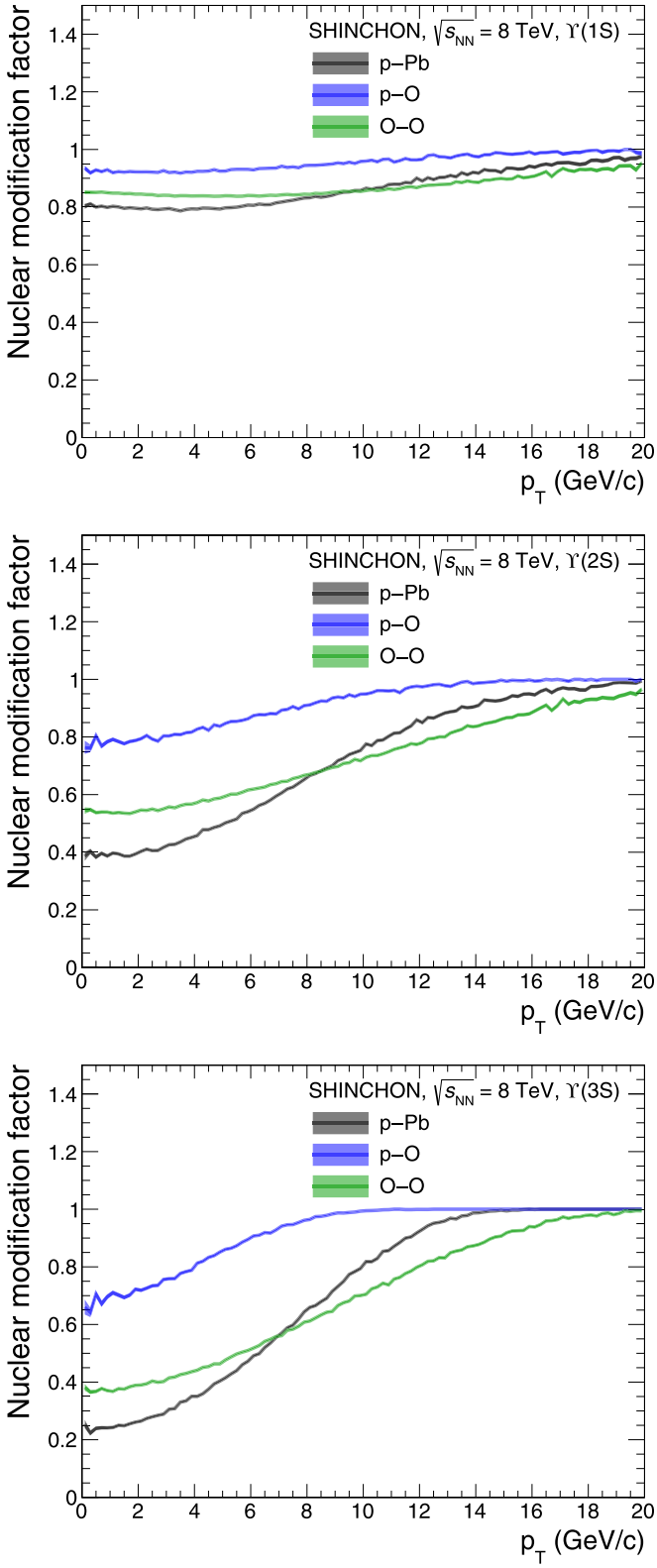


FIG. 10. Nuclear modification factors for $\Upsilon(1S)$, $\Upsilon(2S)$, and $\Upsilon(3S)$ as a function of $p_T$ in $p+\mathrm{O}$, $p+\mathrm{Pb}$, and O+O collisions at $\sqrt{s_{NN}} = 8$ TeV. The uncertainties represent the statistical uncertainty to the corresponding simulated events.

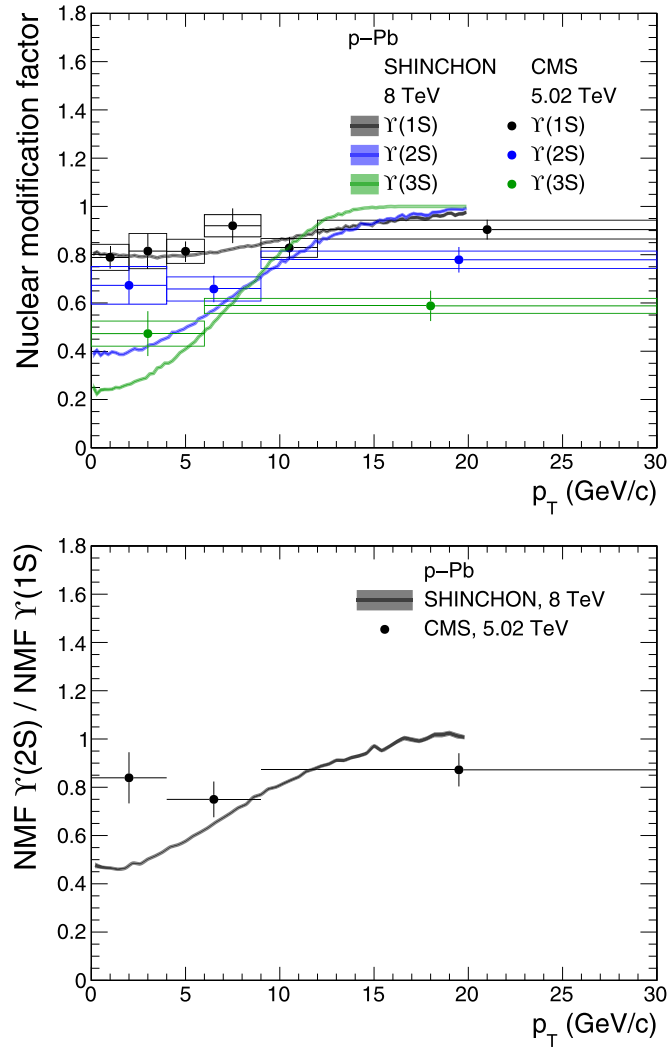


FIG. 11. Calculated nuclear modification factor for $\Upsilon(1S)$, $\Upsilon(2S)$, and $\Upsilon(3S)$ as a function of $p_T$ in $p+\mathrm{Pb}$ collisions at $\sqrt{s_{NN}} = 8$ TeV compared with the CMS results at $\sqrt{s_{NN}} = 5.02$ TeV, and the ratio of nuclear modification factors between $\Upsilon(1S)$ and $\Upsilon(2S)$.

in Fig. 12. For all three $\Upsilon$ states, the $v_2$ values are consistent with zero in the overall $p_T$ region in $p+\mathrm{Pb}$, $p+\mathrm{O}$, and O+O collisions. Also, their $v_2$ values are very similar among the three collision systems. It may indicate that the elongated formation time of $\Upsilon$'s towards high $p_T$ is not as significant as that implemented in the employed model. To test the relation between $v_2$ and the amount of suppression, we computed $v_2$ in 0–5% selected high-multiplicity events as shown in Fig. 13. For all $\Upsilon$ states, the $v_2$ values are found to be larger at high multiplicity only with a small magnitude.

Although the yields of $\Upsilon$ mesons are more strongly suppressed for excited states as well as for higher multiplicity events, their $v_2$ values show an overall consistency with each other in all studied cases. In particular, since the low-$p_T$ $\Upsilon$ mesons are traversing very slowly, it is expected to be unlikely

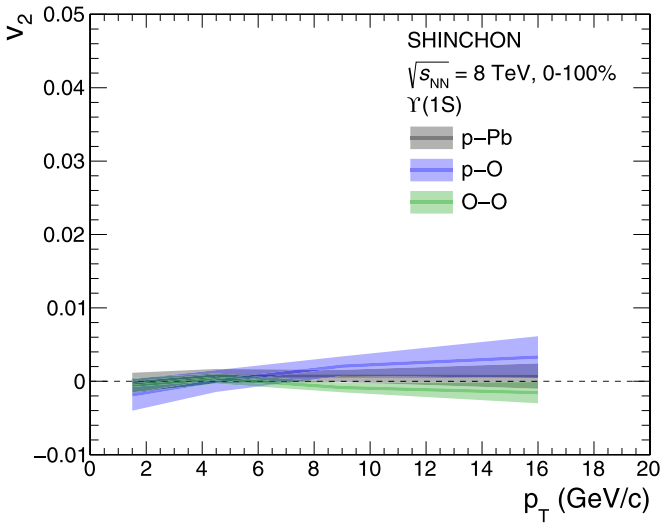


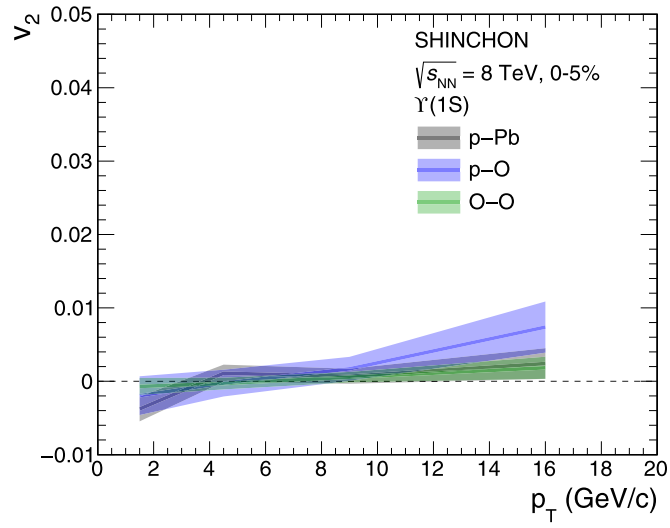


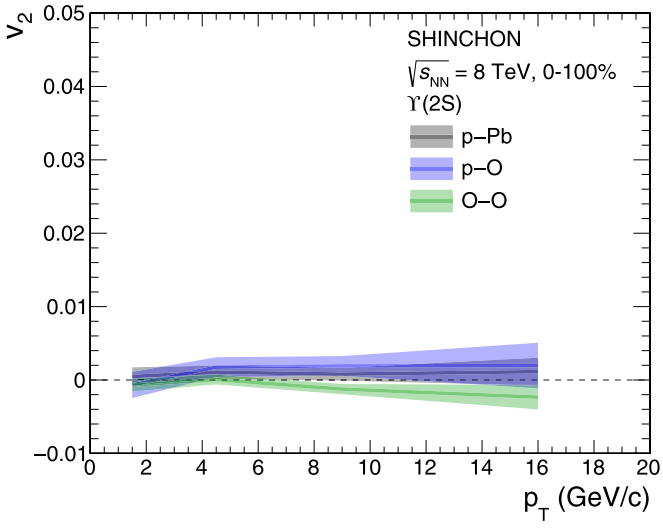


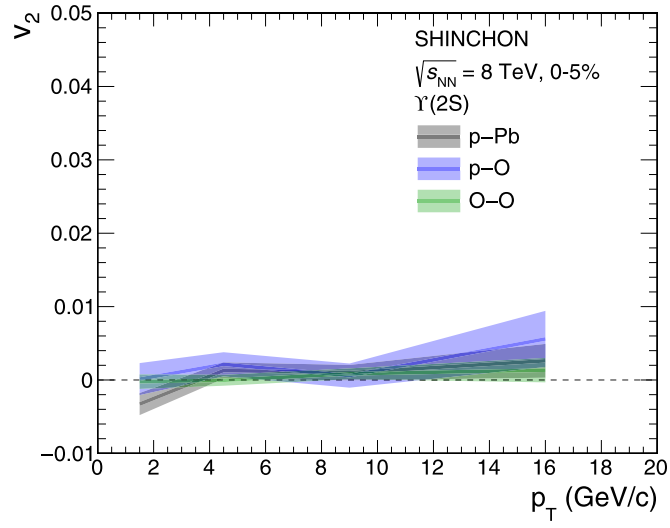


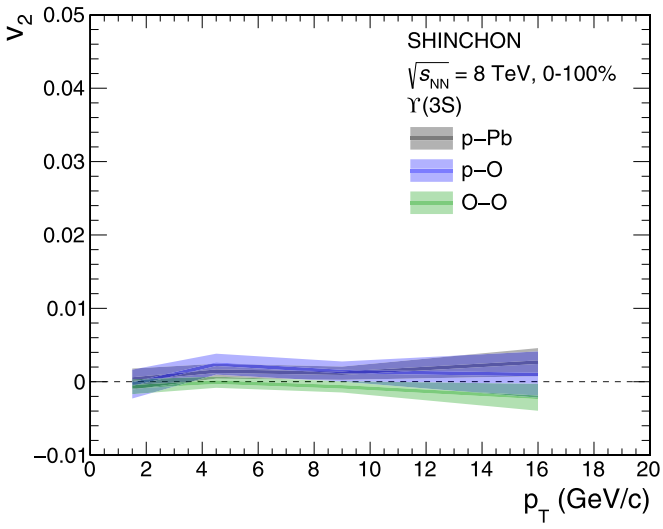


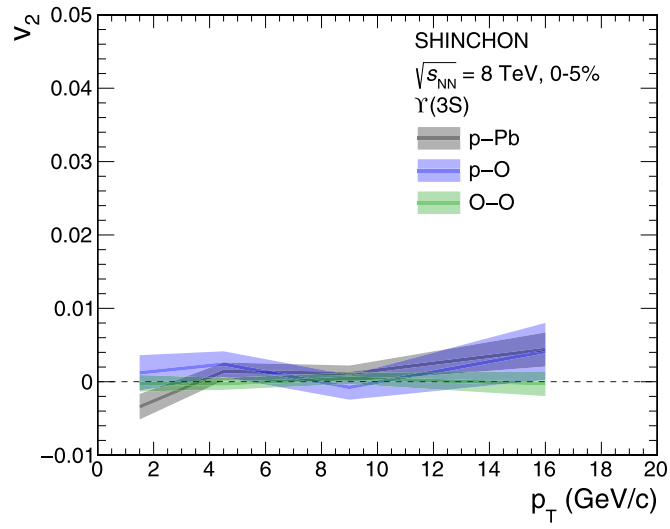


FIG. 12. Calculated $v_2$ in $p$ + Pb, $p$ + O, and O+O collisions as a function of $p_T$ for $\Upsilon(1S)$ (top), $\Upsilon(2S)$ (middle), $\Upsilon(3S)$ (bottom) at $\sqrt{s_{NN}} = 8$ TeV. The uncertainties represent the statistical uncertainty to the corresponding simulated events.

FIG. 13. Calculated $v_2$ in $p$ + Pb, $p$ + O, and O+O collisions as a function of $p_T$ for $\Upsilon(1S)$ (top), $\Upsilon(2S)$ (middle), $\Upsilon(3S)$ (bottom) at $\sqrt{s_{NN}} = 8$ TeV in 0–5% high multiplicity events. The uncertainties represent the statistical uncertainty to the corresponding simulated events.

that they escape the medium before it reaches the chemical freeze-out temperature. Therefore, such $\Upsilon$ mesons are not able to capture the anisotropy of the initial collision geometry despite their significant suppression. It is understood that the path-length dependent suppression could lead to a nonzero $v_2$ which can be probed at high $p_T$ for $\Upsilon$ mesons. However, with our current simulation settings, we did not observe any firm nonzero $v_2$ that deviates from that at low $p_T$ in small collision systems for all $\Upsilon$ states.

## IV. SUMMARY

We performed a Monte Carlo simulation study for the medium response of bottomonia in $p+A$ and $A+A$ collisions. The simulation framework was developed based on the theoretical calculation of the thermal width of $\Upsilon(nS)$ [39] and the publicly available codes to describe the initial condition and evolution of heavy-ion collisions. In this initial work, only the dissociation effect was considered, and we also considered the contribution of feed-down from higher excited states. To demonstrate the framework, we calculated the nuclear modification factor and elliptic flow of $\Upsilon(nS)$ and compared to experimental results. In the nuclear modification factor as a function of the number of participants, the model and data are comparable for $\Upsilon(1S)$ at the entire region, whereas the suppressions for $\Upsilon(2S)$ and $\Upsilon(3S)$ are stronger in the model. In addition to the formation time, which could directly affect the magnitude of nuclear modification, the comparison for excited states would be improved when incorporating the regeneration effect. In case of the elliptic flow, the model expects $v_2 < 0.01$, which agrees with the experimental results [57,58].

We extended the framework to small systems, $p+\mathrm{Pb}$, $p+\mathrm{O}$, and O+O collisions at $\sqrt{s_{NN}} = 8$ TeV. Generally, a stronger modification is observed for higher states ($R^{\Upsilon(1S)}_{pA,AA} > R^{\Upsilon(2S)}_{pA,AA} > R^{\Upsilon(3S)}_{pA,AA}$) even in small systems. In low multiplicity events where the system size is very small, less suppression of $\Upsilon(3S)$ is observed due to the late formation time. In comparing different systems at the same multiplicity, a similar suppression is seen in $dN_{ch}/d\eta < 25$. At higher multiplicity, the modification in O+O is weaker than that in $p+\mathrm{Pb}$ because the energy density (temperature) in O+O is lower due to the larger system size. Regarding the elliptic flow results, we obtained very small (<0.01) elliptic flow for all three systems, even in high multiplicity events. It will be very interesting to compare with experimental results from the upcoming LHC run with the oxygen ion. It can provide valuable information on sources of nuclear effects on bottomonia production in small systems.

## ACKNOWLEDGMENTS

The work was supported by a National Research Foundation of Korea (NRF) grant funded by the Korea government (MSIT) under Projects No. 2018R1A5A1025563, No. 2020R1C1C1004985, and No. NRF-2008-00458. We also acknowledge technical support from KIAF administrators at KISTI.

[1] W. Busza, K. Rajagopal, and W. van der Schee, Heavy ion collisions: The big picture, and the big questions, Annu. Rev. Nucl. Part. Sci. **68**, 339 (2018).
[2] F. Karsch, E. Laermann, and A. Peikert, The Pressure in 2, 2+1 and 3 flavour QCD, Phys. Lett. B **478**, 447 (2000).
[3] E. V. Shuryak, Theory of hadronic plasma, Zh. Eksp. Teor. Fiz. **74**, 408 (1978) [Sov. Phys. JETP **47**, 212 (1978)].
[4] T. Matsui and H. Satz, $J/\psi$ suppression by quark-gluon plasma formation, Phys. Lett. B **178**, 416 (1986).
[5] S. Digal, P. Petreczky, and H. Satz, Quarkonium feed down and sequential suppression, Phys. Rev. D **64**, 094015 (2001).
[6] M. Laine, O. Philipsen, P. Romatschke, and M. Tassler, Real-time static potential in hot QCD, J. High Energy Phys. 03 (2007) 054.
[7] N. Brambilla, J. Ghiglieri, A. Vairo, and P. Petreczky, Static quark antiquark pairs at finite temperature, Phys. Rev. D **78**, 014017 (2008).
[8] N. Brambilla, M. A. Escobedo, J. Ghiglieri, J. Soto, and A. Vairo, Heavy quarkonium in a weakly coupled quark-gluon plasma below the melting temperature, J. High Energy Phys. 09 (2010) 038.
[9] M. I. Gorenstein, A. P. Kostyuk, H. Stoecker, and W. Greiner, Statistical coalescence model with exact charm conservation, Phys. Lett. B **509**, 277 (2001).
[10] A. Andronic, P. Braun-Munzinger, K. Redlich, and J. Stachel, Evidence for charmonium generation at the phase boundary in ultra-relativistic nuclear collisions, Phys. Lett. B **652**, 259 (2007).
[11] L. Ravagli and R. Rapp, Quark coalescence based on a transport equation, Phys. Lett. B **655**, 126 (2007).
[12] J.-P. Blaizot, D. De Boni, P. Faccioli, and G. Garberoglio, Heavy quark bound states in a quark-gluon plasma: Dissociation and recombination, Nucl. Phys. A **946**, 49 (2016).
[13] L. Adamczyk *et al.* (STAR Collaboration), Suppression of $\Upsilon$ production in d+Au and Au+Au collisions at $\sqrt{s_{NN}} =$ 200 GeV, Phys. Lett. B **735**, 127 (2014).
[14] A. M. Sirunyan *et al.* (CMS Collaboration), Measurement of prompt and nonprompt charmonium suppression in PbPb collisions at 5.02 TeV, Eur. Phys. J. C **78**, 509 (2018).
[15] M. Aaboud *et al.* (ATLAS Collaboration), Prompt and nonprompt $J/\psi$ and $\psi(2S)$ suppression at high transverse momentum in 5.02 TeV Pb+Pb collisions with the ATLAS experiment, Eur. Phys. J. C **78**, 762 (2018).
[16] A. M. Sirunyan *et al.* (CMS Collaboration), Measurement of nuclear modification factors of $\Upsilon(1S)$, $\Upsilon(2S)$, and $\Upsilon(3S)$ mesons in PbPb collisions at $\sqrt{s_{NN}} = 5.02$ TeV, Phys. Lett. B **790**, 270 (2019).
[17] S. Acharya *et al.* (ALICE Collaboration), Studies of $J/\psi$ production at forward rapidity in PbPb collisions at $\sqrt{s_{NN}} =$ 5.02 TeV, J. High Energy Phys. 02 (2020) 041.
[18] S. Acharya *et al.* (ALICE Collaboration), $\Upsilon$ production and nuclear modification at forward rapidity in Pb-Pb collisions at $\sqrt{s_{NN}} = 5.02$ TeV, Phys. Lett. B **822**, 136579 (2021).

[19] ATLAS Collaboration, Production of $\Upsilon$(nS) mesons in Pb+Pb and $pp$ collisions at 5.02 TeV, arXiv:2205.03042

[20] CMS Collaboration, Observation of the $\Upsilon$(3S) meson and sequential suppression of $\Upsilon$ states in PbPb collisions at $\sqrt{s_{\rm NN}} =$ 5.02 TeV, CERN Technical Report No. CMS-PAS-HIN-21-007, 2022 (unpublished).

[21] R. Vogt, Shadowing effects on $J/\psi$ and $\Upsilon$ production at energies available at the CERN Large Hadron Collider, Phys. Rev. C **92**, 034909 (2015).

[22] Fr. Arleo and S. Peigné, Quarkonium suppression from coherent energy loss in fixed-target experiments using LHC beams, Adv. High Energy Phys. **2015**, 961951 (2015).

[23] D. C. McGlinchey, A. D. Frawley, and R. Vogt, Impact parameter dependence of the nuclear modification of $J/\psi$ production in $d+$Au collisions at $\sqrt{S_{NN}} = 200$ GeV, Phys. Rev. C **87**, 054910 (2013).

[24] F. Arleo, P. B. Gossiaux, T. Gousset, and J. Aichelin, Charmonium suppression in $p$–$A$ collisions, Phys. Rev. C **61**, 054906 (2000).

[25] A. Capella, A. Kaidalov, A. Kouider Akil, and C. Gerschel, $J\psi$ and $\psi'$ suppression in heavy ion collisions, Phys. Lett. B **393**, 431 (1997).

[26] E. G. Ferreiro, Excited charmonium suppression in proton–nucleus collisions as a consequence of comovers, Phys. Lett. B **749**, 98 (2015).

[27] E. G. Ferreiro and J.-P. Lansberg, Is bottomonium suppression in proton-nucleus and nucleus-nucleus collisions at LHC energies due to the same effects? J. High Energy Phys. 10 (2018) 094; 03 (2019) 063.

[28] V. Khachatryan *et al.* (CMS Collaboration), Observation of long-range, near-side angular correlations in proton-proton collisions at the LHC, J. High Energy Phys. 09 (2010) 091.

[29] G. Aad *et al.* (ATLAS Collaboration), Observation of Long-Range Elliptic Azimuthal Anisotropies in $\sqrt{s} = 13$ and 2.76 TeV $pp$ Collisions with the ATLAS Detector, Phys. Rev. Lett. **116**, 172301 (2016).

[30] V. Khachatryan *et al.* (CMS Collaboration), Evidence for collectivity in pp collisions at the LHC, Phys. Lett. B **765**, 193 (2017).

[31] S. Acharya *et al.* (ALICE Collaboration), Long- and short-range correlations and their event-scale dependence in high-multiplicity pp collisions at $\sqrt{s} = 13$ TeV, J. High Energy Phys. 05 (2021) 290.

[32] S. Chatrchyan *et al.* (CMS Collaboration), Observation of long-range near-side angular correlations in proton-lead collisions at the LHC, Phys. Lett. B **718**, 795 (2013).

[33] B. Abelev *et al.* (ALICE Collaboration), Long-range angular correlations on the near and away side in $p$-Pb collisions at $\sqrt{s_{NN}} =$ 5.02TeV, Phys. Lett. B **719**, 29 (2013).

[34] R. Aaij *et al.* (LHCb Collaboration), Measurements of long-range near-side angular correlations in $\sqrt{s_{\rm NN}} = 5$ TeV proton-lead collisions in the forward region, Phys. Lett. B **762**, 473 (2016).

[35] V. Khachatryan *et al.* (CMS Collaboration), Evidence for Collective Multiparticle Correlations in $p$-Pb Collisions, Phys. Rev. Lett. **115**, 012301 (2015).

[36] A. M. Sirunyan *et al.* (CMS Collaboration), Multiparticle correlation studies in $p$Pb collisions at $\sqrt{s_{NN}} =$ 8.16TeV, Phys. Rev. C **101**, 014912 (2020).

[37] L. Adamczyk *et al.* (STAR Collaboration), Long-range pseudorapidity dihadron correlations in $d+$Au collisions at $\sqrt{s_{\rm NN}} = 200$ GeV, Phys. Lett. B **747**, 265 (2015).

[38] C. Aidala *et al.* (PHENIX Collaboration), Creation of quark–gluon plasma droplets with three distinct geometries, Nat. Phys. **15**, 214 (2019).

[39] J. Hong and S. H. Lee, $\Upsilon(1S)$ transverse momentum spectra through dissociation and regeneration in heavy-ion collisions, Phys. Lett. B **801**, 135147 (2020).

[40] P. Romatschke, Light-heavy ion collisions: A window into pre-equilibrium QCD dynamics? Eur. Phys. J. C **75**, 305 (2015).

[41] S. H. Lim, J. Carlson, C. Loizides, D. Lonardoni, J. E. Lynn, J. L. Nagle, J. D. Orjuela Koop, and J. Ouellette, Exploring new small system geometries in heavy ion collisions, Phys. Rev. C **99**, 044904 (2019).

[42] M. L. Miller, K. Reygers, S. J. Sanders, and P. Steinberg, Glauber modeling in high energy nuclear collisions, Annu. Rev. Nucl. Part. Sci. **57**, 205 (2007).

[43] M. Aaboud *et al.* (ATLAS Collaboration), Measurement of the total cross section from elastic scattering in pp collisions at $\sqrt{s} =$ 8TeV with the ATLAS detector, Phys. Lett. B **761**, 158 (2016).

[44] A. M. Sirunyan *et al.* (CMS Collaboration), Pseudorapidity distributions of charged hadrons in proton-lead collisions at $\sqrt{s_{NN}} =$ 5.02 and 8.16 TeV, J. High Energy Phys. 01 (2018) 045.

[45] S. Acharya *et al.* (ALICE Collaboration), Charged-particle pseudorapidity density at mid-rapidity in p-Pb collisions at $\sqrt{s_{\rm NN}} =$ 8.16 TeV, Eur. Phys. J. C **79**, 307 (2019).

[46] J. S. Moreland, J. E. Bernhard, and S. A. Bass, Alternative ansatz to wounded nucleon and binary collision scaling in high-energy nuclear collisions, Phys. Rev. C **92**, 011901(R) (2015).

[47] B. Schenke, P. Tribedy, and R. Venugopalan, Fluctuating Glasma Initial Conditions and Flow in Heavy Ion Collisions, Phys. Rev. Lett. **108**, 252301 (2012).

[48] C. Bierlich *et al.*, A comprehensive guide to the physics and usage of PYTHIA 8.3, SciPost Phys. Codebases **8** (2022).

[49] A. Mocsy, P. Petreczky, and M. Strickland, Quarkonia in the quark gluon plasma, Int. J. Mod. Phys. A **28**, 1340012 (2013).

[50] H. Satz, Colour deconfinement and quarkonium binding, J. Phys. G: Nucl. Part. Phys. **32**, R25 (2006).

[51] X. Du, M. He, and R. Rapp, Color screening and regeneration of bottomonia in high-energy heavy-ion collisions, Phys. Rev. C **96**, 054901 (2017).

[52] V. Khachatryan *et al.* (CMS Collaboration), Measurements of the $\Upsilon$(1S), $\Upsilon$(2S), and $\Upsilon$(3S) differential cross sections in pp collisions at $\sqrt{s} = 7$ TeV, Phys. Lett. B **749**, 14 (2015).

[53] R. Aaij *et al.* (LHCb Collaboration), Forward production of $\Upsilon$ mesons in $pp$ collisions at $\sqrt{s} = 7$ and 8 TeV, J. High Energy Phys. 11 (2015) 103.

[54] R. Aaij *et al.* (LHCb Collaboration), Study of $\chi_b$ meson production in $pp$ collisions at $\sqrt{s} = 7$ and 8 TeV and observation of the decay $\chi_b(3P) \to \Upsilon(3S)\gamma$, Eur. Phys. J. C **74**, 10 (2014).

[55] P. A. Zyla *et al.* (Particle Data Group), Review of particle physics, Prog. Theor. Exp. Phys. **2020**, 083C01 (2020).

[56] N. Brambilla, H. S. Chung, and A. Vairo, Inclusive production of heavy quarkonia in pNRQCD, J. High Energy Phys. 09 (2021) 032.

[57] S. Acharya *et al.* (ALICE Collaboration), Measurement of $\Upsilon$(1S) Elliptic Flow at Forward Rapidity in Pb-Pb Collisions at $\sqrt{s_{NN}} = 5.02$ TeV, Phys. Rev. Lett. **123**, 192301 (2019).

[58] A. M. Sirunyan *et al.* (CMS Collaboration), Measurement of the azimuthal anisotropy of $\Upsilon$(1S) and $\Upsilon$(2S) mesons in PbPb collisions at $\sqrt{s_{NN}} = 5.02$ TeV, Phys. Lett. B **819**, 136385 (2021).

[59] A. Tumasyan *et al.* (CMS Collaboration), Nuclear modification of $\Upsilon$ states in pPb collisions at $\sqrt{s_{NN}} = 5.02$ TeV, Phys. Lett. B **835**, 137397 (2022).

[60] F. Arleo and S. Peigné, Quarkonium suppression in heavy-ion collisions from coherent energy loss in cold nuclear matter, J. High Energy Phys. 10 (2014) 073.